Kenneth J. Weeks, PhD

Brachytherapy Object-oriented Treatment Planning Based on Three-dimensional Image Guidance[1]

The introduction of radionuclides adjacent to or within regions of tumor in the human body has a long history (1,2). The first such use was reported in 1904. Understanding of the basic biology and the clinical rationale for radium use was the goal of the Paris school (2) just after World War I. Radiation dose prescription was further refined in Manchester, England, in the 1930s (3).

Because the dose and dose rates to some parts of the suspected tumor tissues are high, opportunities for both cure and complications are present in brachytherapy. To define treatments that reach tolerance in normal tissues, guidelines for critical doses to geometrically defined points were developed (3,4). These dose points were defined with fixed rules with regard to the assembly of three-dimensional (3D) information from orthogonal images. On the basis of this geometric information and with the advent of computer planning, the dose distribution is now typically determined in three orthogonal planes to evaluate a brachytherapy implant. Nevertheless, the basic strategy for implantation in a patient has been relatively fixed for many years and is highly dependent on a few point doses (1,2).

Three-dimensional imaging (5) of patient anatomy by means of computed tomography (CT), magnetic resonance (MR) imaging, or ultrasound (US) can now provide far more detailed views of brachytherapy implants. CT is a readily available 3D imaging modality (5). It provides superior geometric accuracy and excellent visualization of normal anatomy. MR imaging has the advantage of providing improved tumor visualization (5). These modalities can be used after the surgical procedure to insert applicators into the body. The planning then concerns the radioactive source loading of the applicator, needles, et cetera, and/or the acceptance of the implant. US has the advantage of providing real-time guidance, which is necessary when placing permanent implants (6). In other words, the step-by-step introduction and acceptance of possible source locations may be achieved in the surgical suite with US.

Recently, improvements in computer hardware and software have facilitated 3D visualization of brachytherapy implants (7). The new imaging advances (relative to plain radiography) now offer the opportunity for improved 3D evaluation of the dose to the tumor and to normal tissues. Nevertheless, brachytherapy procedures require real-time decisions about the radioisotope distribution pattern and other issues. It is possible to organize the 3D data that arise from the imaging information and the physics of the radioisotopes into 3D objects that may be analyzed in a uniform manner. In this chapter, I shall describe the methods used in and present examples of brachytherapy object-oriented treatment planning based on 3D image guidance.

METHODS

In this chapter, CT information is used to illustrate the applications. However, the methods presented may be used for any of the imaging modalities that are available. Throughout this chapter, "contouring an object" in a particular CT section refers to the point-by-point outlining of the boundary of the object in that section.

Objects

All entities in the procedure are classified as objects and, once constructed, are treated geometrically on an equal footing. One can divide the objects into the following three classes: image-based target objects, source-holding structure objects, and dose structure objects.

Image-based target objects.— These objects are defined in terms

RSNA Categorical Course in Brachytherapy Physics 1997; pp 79–86.

[1]From the Department of Radiation Oncology Physics, Duke University Medical Center, Durham, NC.

of their delineation (contouring) on serial sections of the CT data set. A method for constructing a 3D object has been presented by Christiansen and Sederberg (8). These objects include targets to hit (eg, tumor volume, cervix and uterus in carcinoma of the uterine cervix, vaginal wall and vaginal wall plus 5 mm in carcinoma of the vagina, prostate gland in prostate cancer) and targets to miss (eg, rectum, bladder).

Source-holding structure objects.—Radioisotopes are ordinarily deposited into structures that either contain them throughout the duration of the implant or guide their deposition. These objects have a known construction and are sometimes flexible and sometimes of a fixed shape. These objects are defined by their appearance in the imaging data set, their dimensions, or both. Knowledge of the actual shape (dimensions) of the source holders can (*a*) help in correction for distortions in the data set due to patient motion and (*b*) provide precise information on variations in the source material and internal structure orientations.

Dose structure objects.—A matrix of dose or dose rates calculated throughout the geometric region of the implant is also an object. There may be a dose object for each permutation of radioactive source loading produced by the choices of source strength, insertion or deletion of possible source positions, or even radioisotope selection. These objects are the result of calculation of dose in 3D. Examples (1,2) are seed-point dose calculations for iodine-125 or iridium-192 sources, cesium-137 linear sources (either alone or in the presence of high-density material shields), Ir-192 wire sources, and I-125 seed sources with anisotropy corrections.

▮ Planning

Object-oriented decision making involves, first, acquisition of the 3D image data either after or during the implant procedure. One then delineates the anatomy and source-holding structures. This permits reconstruction of solid object representatives of each structure. Selection of calculated dose matrixes to fill each source structure is the next step. The orientation of the dose matrix is required for determining the dose inside the CT coordinate space. A dose rate matrix $D(\mathbf{r}')$ can be calculated for each source-shield-applicator structure referenced to its own intrinsic coordinate system $\mathbf{r}'$. The CT coordinate system is arbitrarily chosen to define the total dose specification coordinate system $\mathbf{r}$.

In general, any solid object is defined in 3D space by using six coordinates (9). A convenient set of coordinates is the object center ($\mathbf{r}_c$) plus the three Euler angles (α, β, γ), which define the rotation of the principal axes of the object. A point p in space (Fig 1) is given in CT space by $\mathbf{r}_p = \mathbf{r}_c + \mathbf{r}_{ps}$, where $\mathbf{r}_c$ is the source center and $\mathbf{r}_{ps}$ is the vector from the source center to point p. The position of p in the source's intrinsic frame is given by the following equation: $E(\alpha, \beta, \gamma)\,(\mathbf{r}_{ps}) = \mathbf{r}'_p$. To determine the Euler matrix E from the image data requires (for the most general case) the referencing of two orthogonal axes for the source structure in the image data. Because, in general, these axes are rotated in CT imaging space (Fig 1), they cannot be directly delineated in the image data. The method used for shielded ovoid source application (10) in carcinoma of the uterine cervix will be presented here to illustrate the indirect imaging of the source axes.

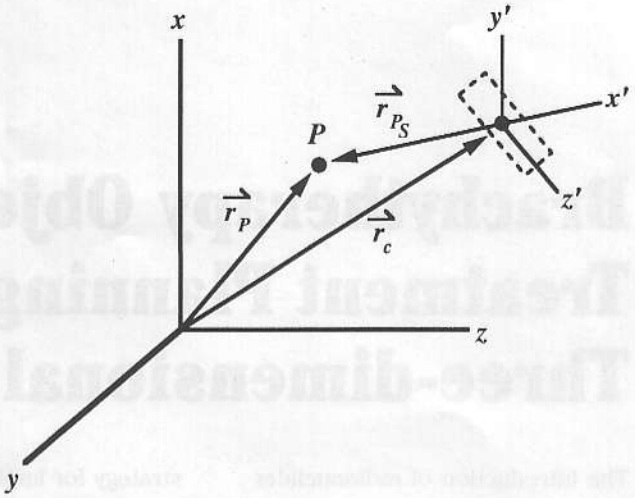

Figure 1. Diagram shows the source object reference frame (x', y', z') and CT coordinate system (x, y, z).

The 3D treatment planning process must first start with the identification of the tandem and ovoids components as imaged in the CT scan set. From this, the relative positions of the sources and shields must be determined. The reality of serial CT imaging is that each section shows a volume averaging of electron density over a given section thickness (5). Identifiable high-attenuation marks on any image section do not necessarily imply that the opaque material lies at exactly that pixel position. Each pixel represents a voxel of material. In fact, even if the section thickness is very narrow, small errors in digitization, patient motion, or both can still make direct interpretation difficult. Thus, it has been found to be easier to have identifiable markers to orient the objects in an indirect manner—namely, one in which the source positions are calculated from information provided by average properties of the structure in

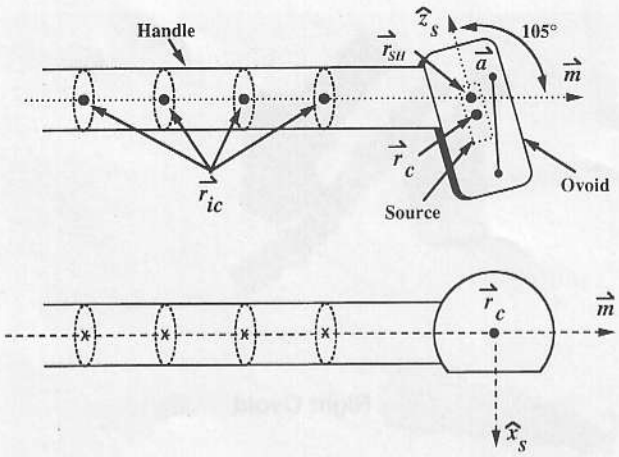

Figure 2. Diagram of a radioactive source-holding consisting of a handle and an ovoid. On the frontal view (top), $\boldsymbol{m}$ is a vector along the axis of the source handle, and $\boldsymbol{a}$ is a vector in the flat side face of the ovoid. On the top view (bottom) of the colpostat, the unit vectors $\boldsymbol{x}_s$ and $\boldsymbol{z}_s$ define the source-intrinsic x and z axes.

the set of CT scans. This information and the known construction of the applicator yield the source coordinates. The problem, as defined here, is to start with a set of source and applicator components, wherein the intrinsic axes of the source in the applicator are initially aligned with the CT axes, and then find the transformation that translates and rotates the source and applicator in 3D such that the source and applicator lies in the position and orientation that it has in the CT data.

One solution is to create a 3D representation of the applicator in the patient from the CT scans and translate and rotate a perfect solid model of the applicator into as close a coincidence as possible to the reconstructed applicator from the imaging data space. Alternatively, or in addition, a method to calculate analytically the sought-for transformation from the CT data–based contouring procedure (and aided by knowledge of the dimensions of the applicator) is useful for saving time.

▮ 3D Asymmetric Source

To illustrate the latter, consider the case of a standard Cs-137 tube source that has been loaded into the ovoid of a Fletcher-type applicator (10). The colpostat is shown schematically in Figure 2. It consists of a handle and an ovoid (which refers to the end of the colpostat that holds the source). One must find not only the center of the source and the orientation of its symmetry axis, but also the x and y axes of the source-holding cavity in the ovoid. The latter is necessary to determine the orientation of the asymmetric dose distribution (produced by the axially symmetric distribution of radioactive material in the source plus the asymmetric distribution of high-density tungsten material in the shield [10]).

For ease of discussion, the serial sections of the CT scan set define the z axis of our coordinate system. The first step is to estimate the CT z coordinate of the source-handle intersection (denoted as $r_{SH}[z]$). This may be estimated to within a millimeter or so with a scout image. The next step is to calculate, from the drawn outlines of the colpostat handles (loops in Fig 2), the centers of these outlines ($\boldsymbol{r}_{ic}$). An average direction cosine $\boldsymbol{m}$ is calculated with the following equation:

$$\boldsymbol{m} = 2\sum_{i=1}^{N-1}\sum_{j>1}^{N}\frac{r_{i_c} - r_{j_c}}{\left|r_{i_c} - r_{j_c}\right| N(N-1)}, \quad (1)$$

The average of the handle centers $\boldsymbol{r}_{AVG}$ is defined by

$$\boldsymbol{r}_{AVG} = \sum_{i=1}^{N} \boldsymbol{r}_{ic} / N. \quad (2)$$

The source handle intersection r_{SH} is then given by

$$\boldsymbol{r}_{SH} = r_{AVG} + \boldsymbol{m}\frac{(r_{SH}[z] - r_{AVG}[z])}{m(z)}, \quad (3)$$

where $r_{AVG}(z)$ and $m(z)$ are the z components of $\boldsymbol{r}_{AVG}$ and $\boldsymbol{m}$, respectively. Another criterion is that the angle between $\boldsymbol{m}$ and the source symmetry axis be 105° (Fig 2). The next construction information is that the distance from the source center to the source handle intersection is 4 mm. Last, the x axis of the asymmetric source is perpendicular to the flat side of the ovoid. One therefore outlines a line a in the flat side of the ovoid in any CT section wherein the flat side of the ovoid is in full view. Therefore, the flat side line is contoured (call it vector $\boldsymbol{a}$). The unit vector along the x axis of the source $\hat{x}_s$ may be determined with the following equation:

$$\hat{x}_S = \frac{\boldsymbol{a} \times \boldsymbol{m}}{|\boldsymbol{a}||\boldsymbol{m}|}. \quad (4)$$

The equations for the source center and the transformation matrix can now be derived from this information and are given in the Appendix.

Therefore, to summarize, from the outlines of the applicator ovoids, the z estimate from the scout scan, and the outline of a line anywhere on the flat side of the ovoid, one can completely determine the three coordinates of the source center and the three Euler

angles needed to bring the source and applicator into alignment with its image in the CT scan set. Note that no single point is directly identified except for the source-handle z coordinate estimate.

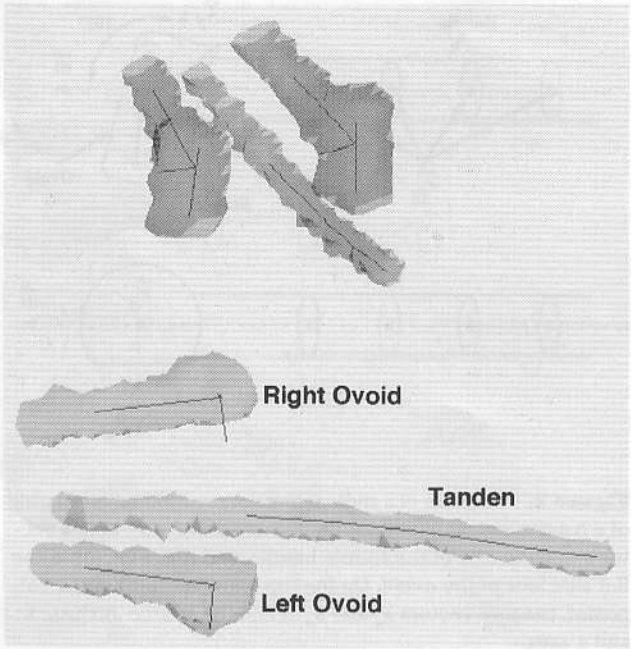

Figure 3. Frontal view of a 3D reconstructed CT scan (top) of the tandem and ovoid objects shows the reconstructed vectors $\boldsymbol{m}$, $\boldsymbol{x}_S$, and $\boldsymbol{z}_S$ as three intersecting lines in the ovoid. Four source symmetry axis lines are connected together in the tandem. Top view (bottom) shows perpendicularity of the x_S axes to their respective ovoid flat surfaces.

RESULTS

Clinical data have been used to test the method. In Figure 3, two views of a clinical case are shown. The tandem source dose matrix is approximately axially symmetric; hence, determination of axes perpendicular to the longitudinal axis is unnecessary. These axes are not shown in Figure 3. Note that the four tandem sources are connected together and are centered in the tandem as they should be. The lower half of Figure 3 shows that the x axes for both the left and right ovoids are perpendicular to their flat faces. Figure 3 depicts good agreement for the solid surface reconstruction and the method described herein. The 3D display of all objects (Fig 3) provides a quick quality assurance check of all aspects of the CT outlining procedure (ie, careless mistakes are magnified at reconstruction). The procedure has been found to be quick, easy, and fairly accurate. The only adjustment needed to date clinically (30 cases) is to adjust the z estimate of the source handle intersection point by no more than 2 mm. Because a 3-mm CT section separation is used, this adjustment is reasonable. After one makes a first guess of this position and the result has been visualized as in Figure 3, reentering a new guess of this coordinate is a straightforward process; after that, it is rare that a second guess is needed. Whether such fine tuning is necessary is determined in seconds by rotating the objects in Figure 3 through several views.

The result of this process (Fig 3) shows that 3D visualization aids in the quick verification of the results. In the example considered, the colpostat itself had high attenuation (10) and was easily visualized with the CT data. Transparent objects would require the introduction of high-attenuating "dummy" materials into the applicator. These dummy markers can be designed to permit reconstruction of the applicator position in a manner analogous to that shown here.

Once the source positions and their orientations have been confirmed, the source strengths may be chosen. The contribution to the dose at any point $D(\boldsymbol{r}_p)$ in the patient is the weighted sum of all the individual source dose matrixes, as follows:

$$D(\boldsymbol{r}_P) = \sum_{i=1}^{N_S} w_i D^i\left(\boldsymbol{r}'_{P_i}\right), \qquad (5)$$

where N_s is the number of sources (each with its own separate coordinate system transformation) and w_i is a source strength in units that depend on the method of dose matrix normalization. By choosing the weighting and calculating the dose over a 3D grid of points, one can display the dose in three ways.

The first method of dose display entails the acquisition of arbitrary sections in the patient and display of the isodose lines on that section. These isodose lines may be superimposed on a calculated CT reconstructed plane as shown in Figure 4. The top half of Figure 4 shows the reconstructed CT section as a 3D object "slicing" through the applicator-anatomy objects. The bottom half of Figure 4 shows the image of the reconstructed section and the point A isodose line, which lies on this image. Note the high-attenuating tandem and ovoid shadows inside the isodose line and compare with the section object visualization in the top half of the figure. This is the traditional presentation of dose (without the CT section). Many isodose lines may be put on the section, or a color wash may be calculated and superimposed on the reconstructed CT section. Finally, note that the section of interest is not an actual CT section but a reconstructed section and that the information used to decide where to best section the object ensues from the same process as the source matrix orientation calculations in the Appendix.

The second method of dose display is the one that we are interested in for the purpose of this chapter. A dose object is created

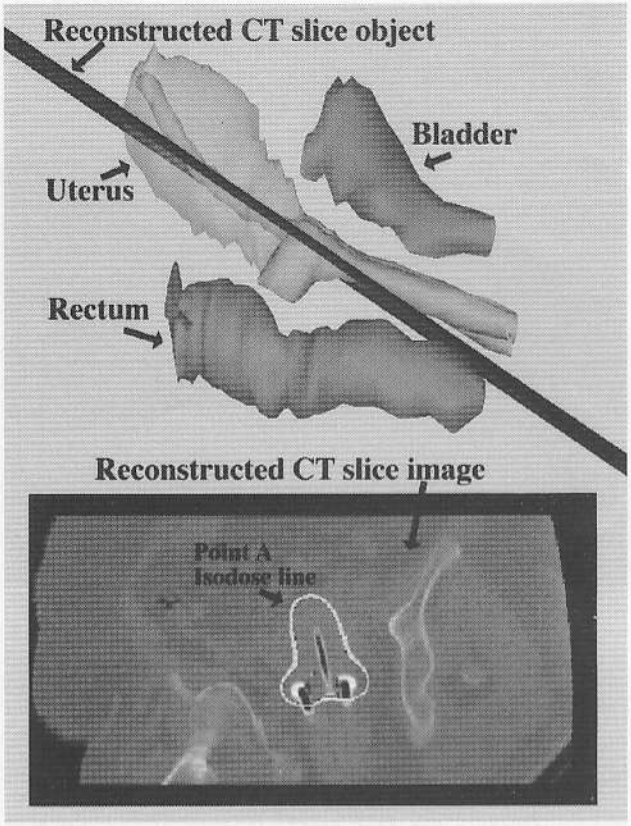

Figure 4. Reconstructed 3D objects from CT sections (top) demonstrate the location of the best coronal-like reconstructed CT section as a geometric object amid organ and applicator objects. Reconstructed CT image (bottom) shows the point A isodose line superimposed over the object.

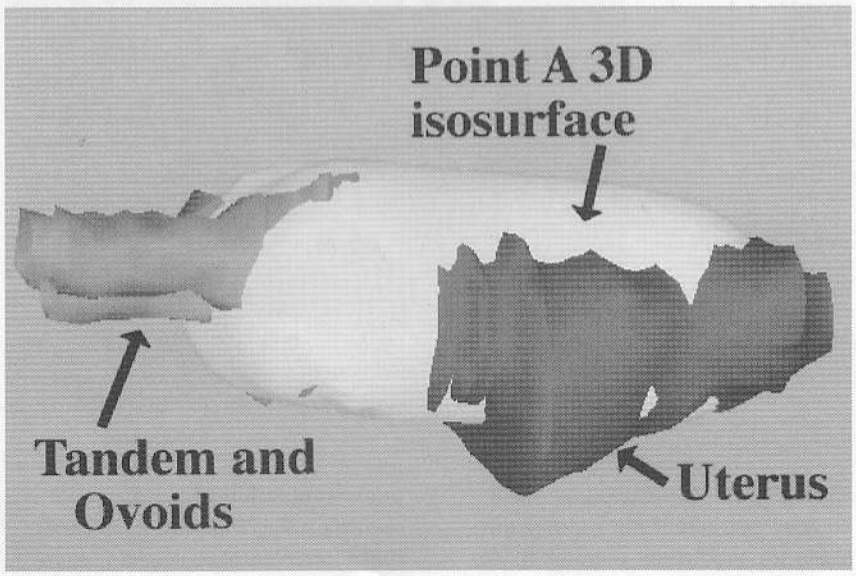

Figure 5. Reconstructed objects from CT scans demonstrate the isosurface solid object coverage of the uterus. The ovoids are partially enclosed by the dose (56 cGy/h) isosurface.

out of a particular 3D isodose surface and is presented along with its relationship to the collection of objects representing the anatomy and the source-holder structure. The creation of such an object is possible with the marching-cube algorithm (11). An example for the treatment of carcinoma of the uterine cervix is shown in Figure 5. Here, an isosurface—the surface in space that goes through the locus of points, all with the special historic (3) point A dose rate—is shown. The relationship of the point A dose rate surface to the uterus indicates that this isosurface easily surrounds the cervix and much of the uterus. Figure 5 also indicates which positions of the uterus have dose rates less than that at point A (ie, the portion of the uterus that is visible in Fig 5). New isosurface dose objects are created in seconds. By selectively choosing different dose isosurfaces to display, one can quickly appreciate the location and magnitude of the hot spots to the rectum and bladder. For example, Figure 6 shows a side view of a 75 cGy/h dose rate isosurface touching the rectum. This indicates the maximum dose to the rectum for this implant. Although it appears that the bladder also intersects the 75 cGy/h surface in Figure 6, rotation to other views shows that the dose rate is a little less. It is clear that 3D display of dose objects can answer all relevant clinical questions in a quick manner.

The third dose presentation scheme is a dose-painted surface object. Figure 7 shows the tandem and ovoids applicator and the patient's rectum and bladder surface dose rates. The outline of the rectum and bladder in the CT data set has been used to generate many points on the surface of the rectum. These geometric points are then formed into a list of points for dose calculation. Each point is converted into a small sphere, and each object's color is determined by color mapping the dose (in Fig 7, black represents a dose rate of greater than 60 cGy/h). So, in fact, there are approximately 1,000 objects in Figure 7. All but three of the objects (namely, the tandem and ovoids) are simple, small spheres. For the example in Figure 7, one notes the large extended contiguous area exposed to dose rates in excess of 60 cGy/h. Appreciation of the area of rectum exposed to any

other chosen level of dose rate is accomplished quickly and easily by simply changing either the color range or gray scale and by changing the viewing angle.

The general treatment planning schema is depicted in Figure 8. The largest time components in Figure 8 are access of the CT data and, especially, contouring of the objects. At our institution, this takes no more than 1.5 hours. Methods to calculate the dose vary in complexity and, hence, time; however, precalculation of source structures is ordinarily clinically acceptable, and, thus, this is not a constraining factor. The rest of the steps in Figure 8 take seconds, except for the issue of evaluation, which, being somewhat subjective, can last any amount of time and will be addressed elsewhere. As mentioned above, the availability of real-time interactive 3D imaging data would allow the feedback at the bottom of Figure 8 to return to the imaging modality, which would enable one to optimize the source-holding structure positions on the basis of how the dose object structures were dynamically changing as sources were added.

Another application is template-guided needle implants for carcinoma of the vagina with the use of strings of Ir-192 seed sources. Brachytherapy object-oriented 3D planning has simple functions such as determining which needles are in or out of the tumor (target to hit) or critical structures (target to miss). Figure 9 shows the 3D anatomy and a 22-needle implant. The vaginal cylinder and the template that guided the needle insertions are shown as objects. The needles inside the rectum or bladder are obvious and thus should not be loaded. In addition, Figure 9 shows that a few needles lie mostly outside the target; the remaining needles are inside the target volume. Creation of a 3D dose object for each needle and selective turning on or off of various combinations quickly enables the treatment planner to decide which needle to load with what length of seed strand. The dose display techniques presented in Figures 5–7 can be used in the same manner.

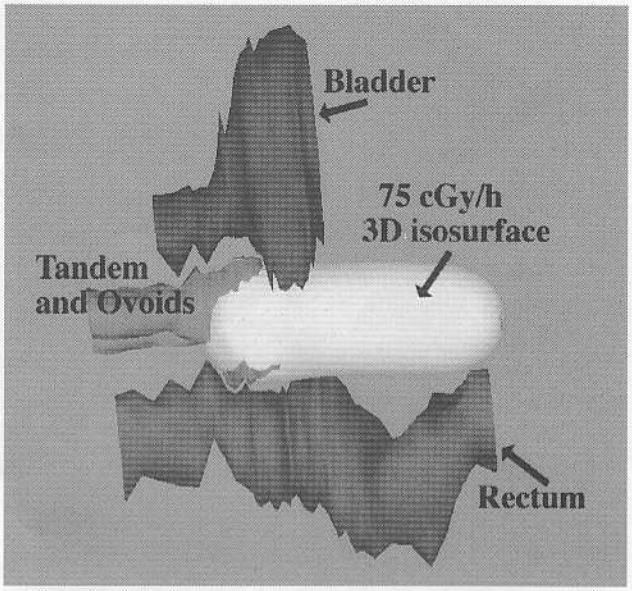

Figure 6. Reconstructed objects from the CT scan and the 75 cGy/h isosurface object (white) for comparison with the rectum and bladder. This view of the object shows the dose isosurface touching the rectum.

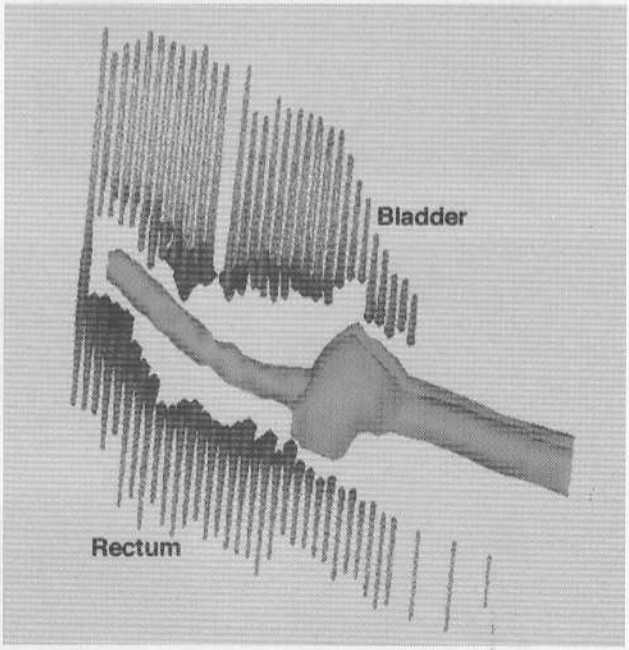

Figure 7. Reconstructed 3D image of dose-shaded rectum and bladder surface points. The darker regions in the rectum and bladder correspond to a dose of at least 60 cGy/h.

Preplan optimization of Ir-192 needle-template implants can be performed quite quickly. Figure 10 shows that creation of a grid object (here viewed from the side) can help in registering the computer simulation of needles (not shown) being implanted. Because these are rotatable objects, rotation to a view along the axis of the physically possible template orientation (ie, where the vaginal cylinder is seen on end) enables one to design a customized template pattern (by using the grid, which rotates with the anatomy objects, to measure the needle-to-needle relationships). During the preplanning stage, straight needles are assumed, the dose distribution is cal-

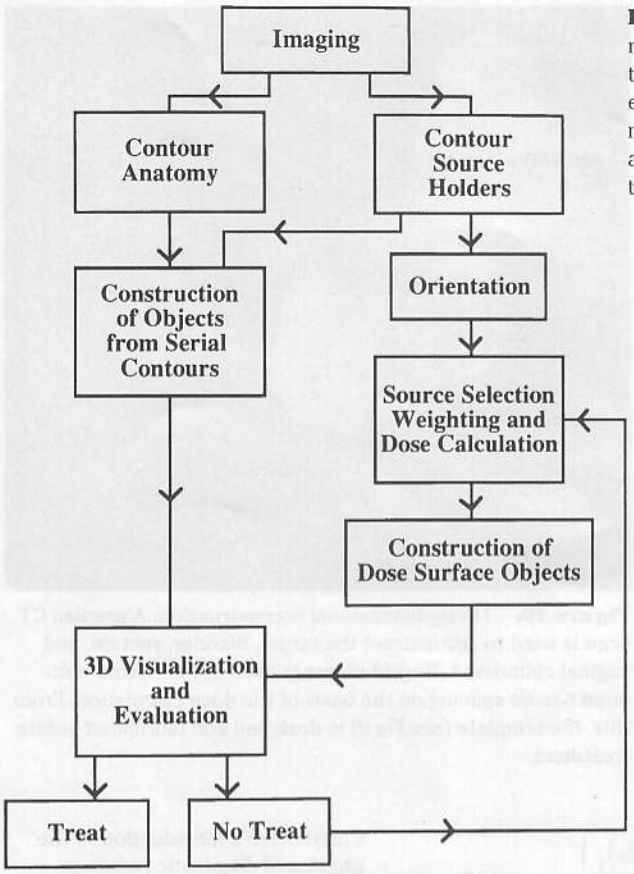

Figure 8. Schematic of the brachytherapy object-oriented treatment planning process. *Treat* = acceptance of the treatment plan.

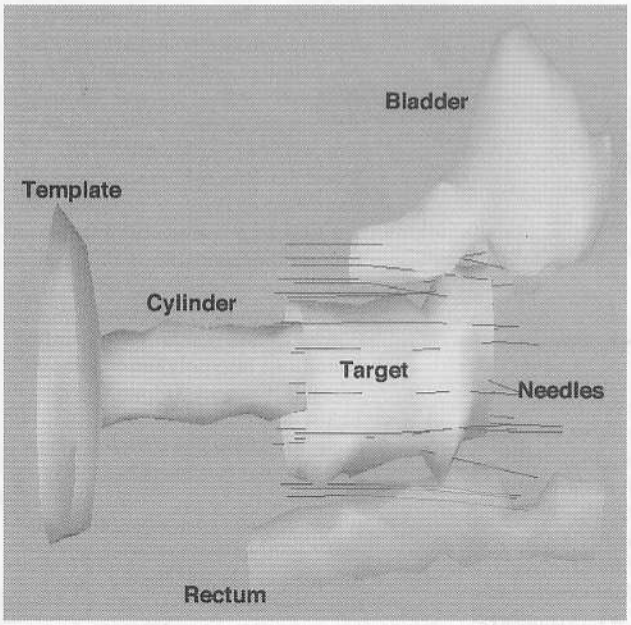

Figure 9. Reconstructed objects from a CT scan for the case of an Ir-192 vaginal template implant. All needles are shown from the tip of their insertion to the most inferior position (left) to which they might be loaded with radioisotopes in order to treat the target volume. The template was used to guide needle insertion.

culated for various-strength loadings of the needles, and the final result of the preplan—namely the number of seed strands, the number of seeds per strand, the strength of sources, and the template design—may be determined. This part of the process uses display techniques similar to those shown in Figures 5–7. The template can then be fabricated with appropriately spaced holes and be made ready for the actual implant procedure.

DISCUSSION

The historic characterization of the 3D dose with a few fixed points has long guided brachytherapy and will continue to be useful. It is clear that 3D dose-surface images have the potential to ameliorate the treatment planning process. With this information, we hope to discover refined therapy guidelines to help the physician avoid generating complications.

Brachytherapy object-oriented 3D treatment planning has been presented as an efficient method for providing improved brachytherapy planning with 3D imaging modalities. Brachytherapy is particularly suited to this imaging development because, even when limited to plain orthogonal radiographs, 3D localization of radioisotopes and 3D representation of the dose as characterized by dose distribution on three orthogonal planes have been standards of practice for many years. Therefore, 3D imaging itself is natural for brachytherapy, and, clearly, the use of CT, MR imaging, and US can improve the reliability of the treatment. Moreover, the acquisition of detailed anatomic dose distribution data and their correlation to subsequent follow-up clinical findings can help us to improve the treatments in the future.

APPENDIX

It is necessary to find the center $\boldsymbol{r}_c$ and the orientation of an object with principal axes characterized by the unit vectors $\boldsymbol{x}_s$ and $\boldsymbol{z}_s$ ($\boldsymbol{y}_s$ is then uniquely defined). The unit vector $\boldsymbol{x}_s$ is given by Equation (4), and $\boldsymbol{r}_{SH}$, $\boldsymbol{m}$, and $\boldsymbol{r}_{AVG}$ have all been defined in the text. The length of the source is denoted by L, and the angle between the source axis and the vector $\boldsymbol{m}$ is θ (105° in reference 10). The distance between points

$\mathbf{r}_{SH}$ and $\mathbf{r}_c$ is t (0.4 cm in reference 10).

Let

$$\mathbf{r}_{AS} \equiv \mathbf{r}_{SH} - \mathbf{r}_{AVG}, \quad \text{(A1)}$$

$$a \equiv \frac{L|\rho_{A\Sigma}|\cos\theta}{e}, \quad \text{(A2)}$$

$$b \equiv \frac{\frac{r_{AS}(x)\hat{x}_S(y)}{\hat{x}_S(x)} + r_{AS}(y)}{e}, \quad \text{(A3)}$$

$$c \equiv fa, \quad \text{(A4)}$$

$$d \equiv (bc/a) - \left[\hat{x}_S(y)/\hat{x}_S(x)\right], \quad \text{(A5)}$$

$$e \equiv r_{AS}(x)f + r_{AS}(z), \quad \text{(A6)}$$

$$f \equiv \left[\hat{x}_S(z)\right]/\left[\hat{x}_S(x)\right], \quad \text{(A7)}$$

$$\Delta y \equiv \frac{-\sqrt{(dc+ab)^2 - \left(1+d^2+b^2\right)\left(c^2+a^2-L^2\right)}}{1+d^2+b^2}, \quad \text{(A8)}$$

$$\Delta z \equiv a - b\Delta y, \quad \text{(A9)}$$

and

$$\Delta x \equiv c - d\Delta y, \quad \text{(A10)}$$

then

$$\hat{z}_S(x) \equiv r_{SH}(x) + \Delta x, \quad \text{(A11)}$$

$$\hat{z}_S(y) \equiv r_{SH}(y) + \Delta y, \quad \text{(A12)}$$

$$\hat{z}_S(z) \equiv r_{SH}(z) + \Delta z. \quad \text{(A13)}$$

The source center coordinates are given by $\mathbf{r}_c = \mathbf{r}_{SH} - t\mathbf{z}_S$. The Euler angles ($\alpha$, β, γ) are given by

$$\alpha = K + \text{atan}\frac{\hat{x}_S(y)}{\hat{z}_S(x)}, \quad \text{(A14)}$$

where $K = 180°$ if $z_s(x) < 0$, $K = 0°$ if $z_s(x) > 0$ and $z_s(y) > 0$, and $K = 360°$ if $z_s(x) > 0$ and $z_s(y) < 0$. Then

$$\beta = \text{acos}\left[\frac{\left(E(\alpha,0,0)\hat{z}_S\right)_z}{\left|E(\alpha,0,0)\hat{z}_S\right|}\right] \quad \text{(A15)}$$

and

$$\gamma = \text{acos}\left[\frac{\left(E(\alpha,\beta,0)\hat{x}_S\right)_x}{\left|E(\alpha,\beta,0)\hat{x}_S\right|}\right]. \quad \text{(A16)}$$

The Euler matrix E is defined in reference 9.

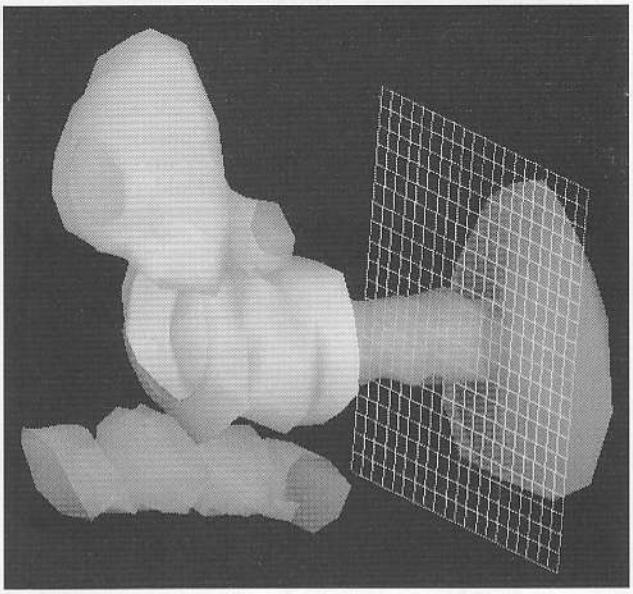

Figure 10. Three-dimensional reconstruction. A preplan CT scan is used to reconstruct the target, bladder, rectum, and vaginal cylinder. A 3D grid object is used to determine optimum needle spacing on the basis of the dose calculation. From this, the template (see Fig 9) is designed and fabricated before treatment.

REFERENCES

1. Glasgow GP, Perez CA. Physics of brachytherapy. In: Perez CA, Brady LW, eds. Principles and practice of radiation oncology. Philadelphia, Pa: Lippincott, 1987; 213–290.
2. Pierquin B, Chassagne DJ, Chahbazian CM, Wilson JF. Brachytherapy. St Louis, Mo: Green, 1978.
3. Tod MC, Meredith WJ. Dosage system for cancer of the cervix. Br J Radiol 1938; 11:809–823.
4. Pierquin B, Dutreix A, Wambersie A, Chassagne D, Stella J. La dosimetrie provisionnele en endocurietherapie (dispositif radifere en un plan: etude sur ordinateur). J Radiol 1969; 50:377–383.
5. Curry TS, Dowdey JF, Murry RC. Christensen's introduction to the physics of diagnostic radiology. Philadelphia, Pa: Lea & Febiger, 1984.
6. Grimm PD, Blasko JC, Ragde H. Ultrasound guided transperineal implantation of iodine-125 and palladium-103 for the treatment of early stage prostate cancer. Atlas Urol Clin North Am 1994; 2:113–125.
7. Weeks KJ. Brachytherapy visualization using AVS. In: Proceedings of the 1994 International AVS Users Group Conference. Boston, Mass: AVS Users Group, 1994; 437–443.
8. Christiansen HN, Sederberg TW. Conversion of complex contour line definitions into polygonal element mosaics. Comput Graphics 1978; 12:187–192.
9. Rose ME. Elementary theory of angular momentum. New York, NY: Wiley, 1957.
10. Weeks KJ, Montana GS. A 3D applicator system for carcinoma of the uterine cervix. Int J Radiat Oncol Biol Phys 1997; 37:455–463.
11. Lorensen WE, Cline HE. Marching cubes: a high resolution 3D surface construction algorithm. Comput Graphics 1987; 21:163–169.